Thin Solid Films 528 (2013) 31–35

Contents lists available at SciVerse ScienceDirect

Thin Solid Films

journal homepage: www.elsevier.com/locate/tsf

# Influence of forming process on resistance switching characteristics of $In_2O_3/SiO_2$ bi-layer

Jheng-Jie Huang [a], Ting-Chang Chang [a,e,*], Po-Chun Yang [b], Yu-Ting Chen [b], Hsueh-Chih Tseng [a], Jyun-Bao Yang [b], Simon M. Sze [a,c,f], Ann-Kuo Chu [b], Ming-Jinn Tsai [d]

[a] Department of Physics, National Sun Yat-Sen University, Kaohsiung 804, Taiwan
[b] Department of Photonics, National Sun Yat-Sen University, Kaohsiung, Taiwan
[c] Institute of Electronics, National Chiao Tung University, Hsin-Chu 300, Taiwan
[d] Electronics and Optoelectronics Research Laboratory, Industrial Technology Research Institute, Chutung, Hsinchu 310, Taiwan
[e] Advanced Optoelectronics Technology Center, National Cheng Kung University, 1 Ta-hsueh Road, Tainan 701, Taiwan
[f] Department of Electrical Engineering, Stanford University, Stanford, CA 94305-4085, USA

ARTICLE INFO

Available online 5 November 2012

*Keywords:*
RRAM
Effect of forming process
Indium diffusion

ABSTRACT

In this study, we fabricated and analyzed resistance switching characteristics for resistance random access memory (RRAM) in a $Pt/In_2O_3/SiO_2/TiN$ structure. By applying opposing electric fields to perform a soft breakdown of the $In_2O_3/SiO_2$ insulating bi-layer, different switching behaviors are exhibited. When positive forming voltage was applied to the TiN electrode to soft breakdown the device, the resistance switching behavior was dominated by the bipolar mode. However, the negative voltage forming process exhibited both unipolar switching characteristics in addition to a bipolar switch mode. In order to analyze the composition of the conduction path and resistance switching mechanism, resistance value trends versus temperature was extracted and showed that the conduction paths of bipolar and unipolar modes are dominated by oxygen vacancies and metallic filament, respectively. Hence, metallic filament was considered to be formed by the migration of indium ions because the unipolar characteristic was only present during negative bias forming condition.



## 1. Introduction

With the development of portable electronic products, sizes of memory devices have been scaled down continuously in order to increase capacity [1–4]. However, traditional nonvolatile floating gate memory has confronted some physical limits because of its complex traditional nonvolatile floating gate structure. In order to solve this problem, resistance random access memory (RRAM) devices have been investigated. RRAM devices have advantages such as low operating consumption, high density (because of simple device structure) and fast switching speed (about several ns) [5,6]. In addition, resistive switching characteristics have been observed in many metal oxides ($Al_2O_3$, NiO, $HfO_2$ ZnO and InGaZnO) [7–16]. Generally, the switching mechanism is due to the formation or rupture of a conduction path composed of oxygen vacancies or metal filament.

## 2. Experiment

In this article, the proposed RRAM device was fabricated on a TiN (500 nm)/$SiO_2$ (20 nm)/Si substrate. On the TiN layer, we deposited a 500 nm low temperature silicon oxide layer and etched a contact hole to define the size of the device and expose the TiN bottom electrode. First, the 10-nm-thick $SiO_2$ and 20-nm-thick $In_2O_3$ layers were sequentially deposited on the TiN electrode layer by RF sputtering the $SiO_2$ and $In_{0.4}O_{0.6}$ target in ambient Ar (30 sccm) at room temperature. Finally, the RRAM device with a $Pt/In_2O_3/SiO_2/TiN$ bi-layer structure was completed after sputtering a 100 nm-thick Pt top electrode on the $In_2O_3$ layer, as shown in inset (i) of Fig. 1. In order to investigate the resistive switching properties of the $In_2O_3/SiO_2$ film, we measured the I–V curves with an Agilent B1500 semiconductor parameter analyzer.

## 3. Results and discussion

During the measurement process, voltage was applied to the TiN electrode while the Pt electrode was grounded, as shown in inset (i) of Fig. 1. In order to form the conduction path, the voltage was swept from 0 V to 10 V, and the resistive switching layer ($In_2O_3/SiO_2$) underwent soft breakdown at about 9.3 V with 1 μA of compliance current, as shown in inset (ii) of Fig. 1. Subsequently, negative voltage was applied to reset the RRAM device. The current decreased when the applied voltage was higher than −0.7 V. After the reset process, the applied voltage was swept from 0 V to 1.5 V with a 10 mA compliance current as the set process. During this set process, the current increased

* Corresponding author at: Department of Physics, National Sun Yat-Sen University, Kaohsiung 804, Taiwan.
*E-mail address:* tcchang@mail.phys.nsysu.edu.tw (T.-C. Chang).

0040-6090/$ – see front matter © 2012 Elsevier B.V. All rights reserved.
http://dx.doi.org/10.1016/j.tsf.2012.10.096

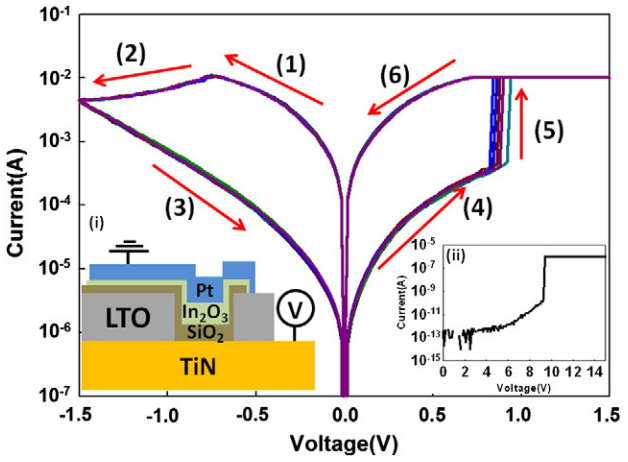


**Fig. 1.** Bipolar switching characteristics of $Pt/In_2O_3/SiO_2/TiN$ structure after positive bias forming process. Inset (i) is the structural diagram of the RRAM device; inset (ii) shows the positive bias forming process.

rapidly until the compliance current was achieved at about 1 V, as shown in Fig. 1.

Therefore, current fitting and the resistance value (R)–temperature (T) measurement were respectively employed to analyze the carrier transport mechanism and the conduction path properties. Fig. 2(a) shows the carrier transport mechanism of the low resistance state (LRS) and that it is dominated by ohmic conduction. Furthermore, this resistance value of the ohmic conduction path decreases with increasing temperature, as shown in Fig. 2(b). This result indicates that the conduction path is composed of oxygen vacancies [17]. Fig. 2(c) shows the carrier transport mechanism of the high resistance state (HRS) and that it is dominated by Frenkel–Poole emission [20].

According to the experiment and analysis, the conduction path forms after forming process because the applied high voltage provides electrons with enough energy to break the metal–oxygen bond (silicon oxide and indium oxide). After the metal–oxygen bond is broken, the oxygen ions migrate to the TiN electrode because of the applied electric field, and the oxygen vacancy conduction path and indium filament are formed in the resistive switching layer, as shown in Fig. 3. Additionally, the oxygen ions which migrate to the TiN electrode combine with Ti and become stored in the TiN electrode [18]. Subsequently, the resistance value increases when the applied voltage is higher than −0.7 V. Due to this applied electric field, the oxygen ions in the TiN electrode are driven to migrate to the resistive switching layer, and then recombine with the vacancy. After the recombination of oxygen ions and vacancies, the conduction path near the TiN interface will be destroyed by the formation of an insulator between the conduction path and TiN. Hence, the carrier transport mechanism is dominated by the Frenkel–Poole emission, as shown in Fig. 2(c). When a higher voltage is applied, more oxygen ions migrate to the resistive switching layer, and the resistance value switches to the high resistance state. Finally, the resistance state can be switched again to low resistance state by applying sufficient positive voltage. The conduction path can be constructed by breaking the metal–oxygen bond by electrons with high energy, as shown in Fig. 3. This switching behavior is repeatable by the cyclical application of the positive/negative voltage, as shown in Fig. 1.

Fig. 4(a) shows the bipolar switching characteristic after the negative bias forming process. After this forming process, the conduction path will be constructed at about −7.9 V and the resistance state will switch to LRS, as shown in inset (i) of Fig. 4(a). Subsequently, the resistance value can be switched to LRS/HRS by applying positive/negative bias, as shown in Fig. 4(a). Inset (ii) of Fig. 4(a) shows the first reset process after the forming process, and an unusual reset behavior was discovered. Compared with the subsequent reset behaviors, the current of the first reset behavior decreases quickly at about −0.8 V, a switching characteristic similar to the reset behavior in unipolar mode [21]. Hence, a higher negative voltage along with the 1 mA compliance current must be applied to the TiN electrode after the first reset process in order to switch the resistive state to LRS, as shown by the blue line in Fig. 4(b). Interestingly, the resistance state can also be switched to HRS by sweeping negative bias afterward, as shown by the red line in Fig. 4(b).

Because this dual switching characteristic exists in this bi-layer RRAM device after the negative bias forming process, the resistance value (R)–temperature (T) curve was measured to clarify the conduction path property and the switching mechanism. The resistance value of LRS induced by a negative bias forming process increases with increasing temperature, as shown in Fig. 5(a). The proportional relationship indicates that the conduction is dominated by the metallic filament. From the direction of the applied electric field, the formation of the conduction path is likely due to the migration of indium ions, causing the unusual first reset process characteristics, as shown in Fig. 5(b). Because the indium ions migrate from the indium oxide layer to the TiN layer, the diameter of the conduction path near the TiN interface is smaller than indium oxide. Hence, a serious joule heating effect will occur surrounding the conduction path near the TiN and will lead the conduction path to rupture immediately, as shown in inset (ii) of Fig. 4(a).

Fig. 6(a) and (b) shows the R–T curves of the bipolar and unipolar modes at LRS. With increasing temperature, the resistance value of the bipolar mode decreases. Hence, the switching mechanism of this bipolar mode is dominated by the formation of oxygen vacancies near the TiN interface, as shown in Fig. 6(c). In the unipolar mode, the conduction path will re-form by using higher negative voltage, and this strong applied electric field will cause a subsequent

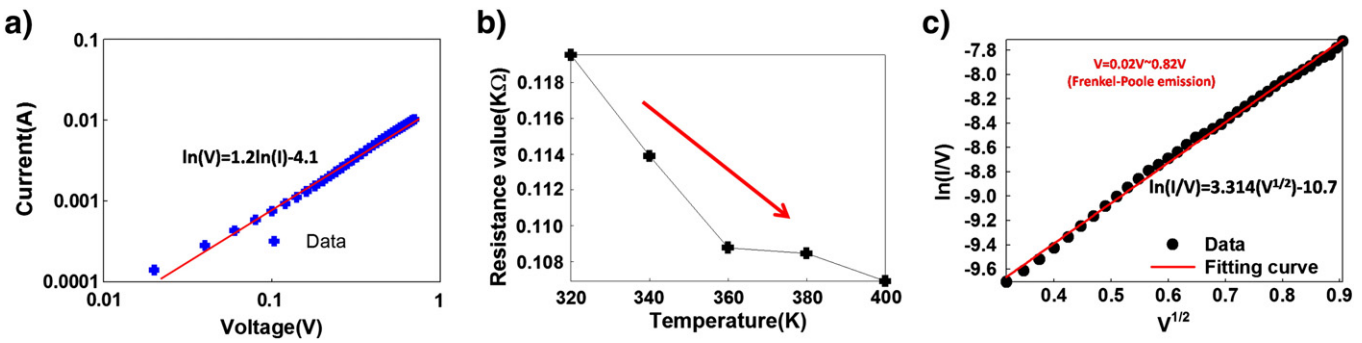


**Fig. 2.** (a) Carrier transport mechanism of LRS, (b) resistance value trends versus temperature for LRS, and (c) carrier transport mechanism for HRS.

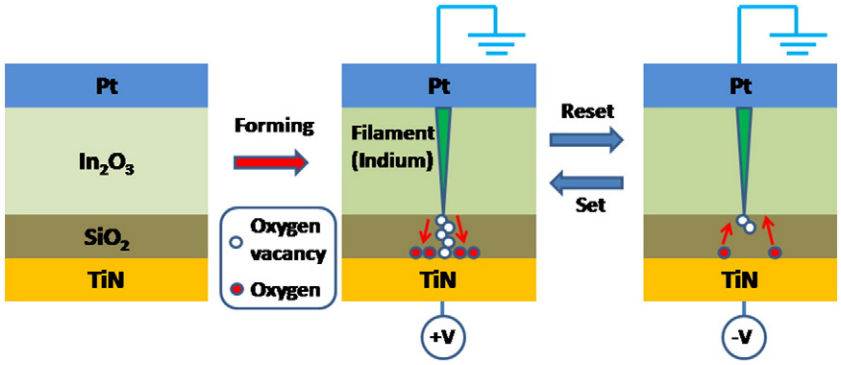


**Fig. 3.** Bipolar switching mechanism diagram of positive bias forming device. The conductive filament is formed by the indium element.

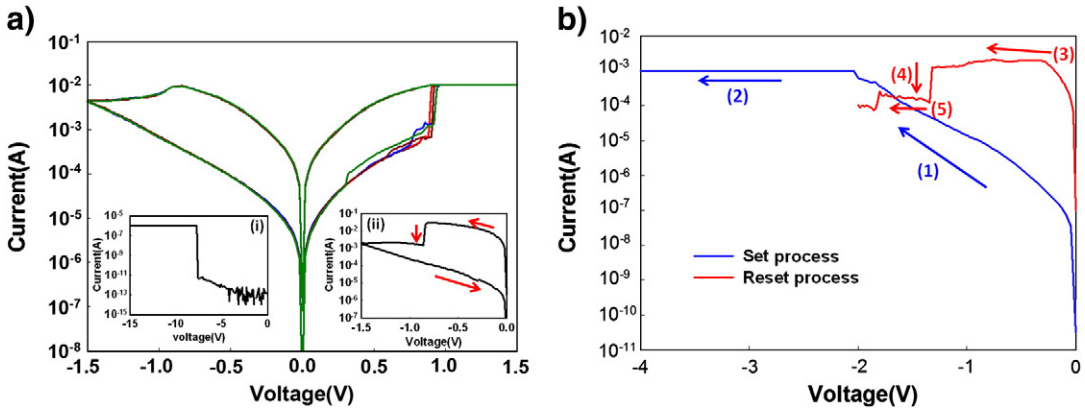


**Fig. 4.** (a) Bipolar and (b) unipolar switching characteristics in the Pt/$In_2O_3$/$SiO_2$/TiN structure after negative bias forming process. Inset (i) shows the negative bias forming process; inset (ii) shows the first reset process.

migration of indium ions. Hence, LRS exhibits a metallic characteristic, and its unipolar mode switching mechanism is dominated by the joule heating effect and the migration of indium ions, as shown in Fig. 6(d).

In addition, we also analyzed the HRS carrier transport mechanism after undergoing soft breakdown by negative bias. Throughout the lower voltage range (0.14 V–0.36 V), the conduction process is Frenkel–Poole emission because some traps or oxygen vacancies existed in the insulator between the conduction path and the TiN electrode, as shown in Fig. 7(a). The Frenkel–Poole emission mechanism was observed both in the positive bias forming device and negative bias forming device. Moreover, the negative bias forming device showed that at higher voltages (0.4 V–0.76 V), the Frenkel–Poole emission mechanism was replaced by the space-charge-limited current (SCLC) mechanism, as shown in Fig. 7(b). This is because the end of the metal filament (the rupture location along the conduction path) induces a strong tip electric field. The band bending near the tip range is very serious due to the strong tip electric field. Hence, the

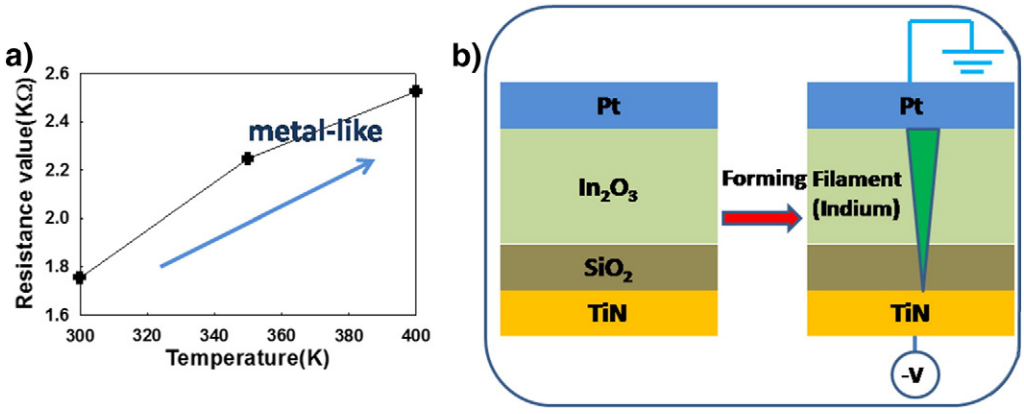


**Fig. 5.** (a) Resistance value with temperature and (b) structural diagram after negative bias forming process.

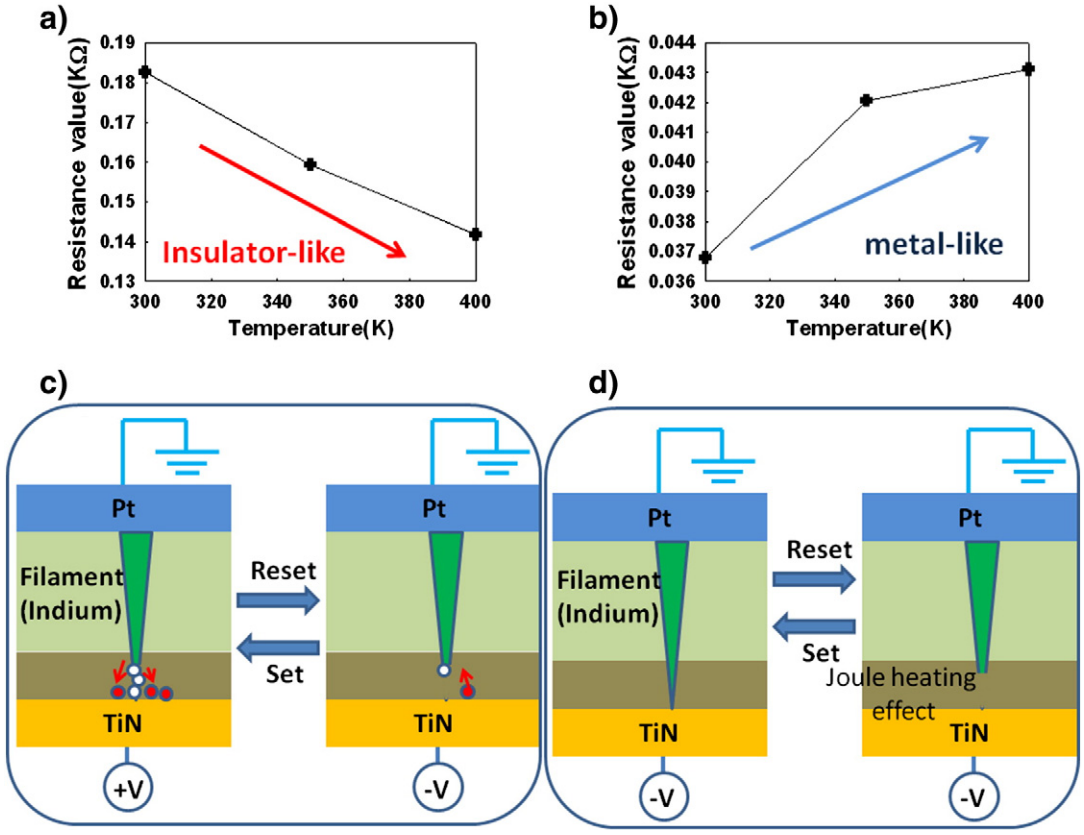


**Fig. 6.** Resistance value (R)–temperature (T) curves of (a) bipolar mode and (b) unipolar mode at LRS. The structural diagram under (c) bipolar and (d) unipolar mode operations after negative bias forming process.

transport of the carrier tunneling into the insulator is limited and thereby produces the SCLC transport mechanism [19], as shown in the inset of Fig. 7(b).

## 4. Conclusion

In summary, an $In_2O_3/SiO_2$ based resistance random access memory (RRAM) device was fabricated with a $Pt/In_2O_3/SiO_2/TiN$ structure. After undergoing two opposite bias forming conditions, these RRAM devices exhibited different switching characteristics. After positive bias forming process, only the bipolar switching mode is observed because the conduction path was formed by oxygen vacancies and the switching mechanism was dominated by their formation. After negative bias forming process, the indium ions migrate into the $SiO_2$ layer and form a metallic conduction path filament. Hence, the negative bias forming device has two kinds of switching characteristics, those of a bipolar mode due to oxygen vacancy formation along the ruptured metal filament as well as a unipolar mode dominated by the formation of an indium filament.

## Acknowledgment

This work was performed at the National Science Council Core Facilities Laboratory for Nano-Science and Nano-Technology in Kaohsiung-Pingtung area and was supported by the National Science Council of the Republic of China under contract no. NSC 100-2120-M-110-003.

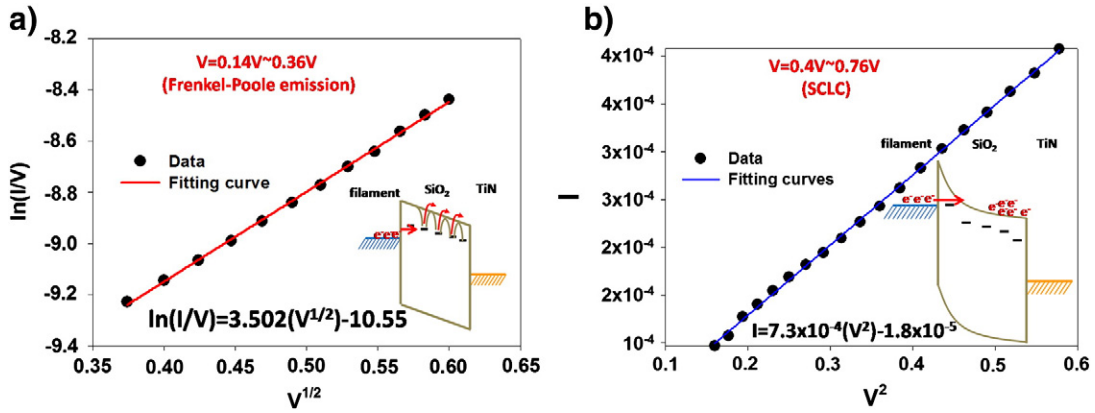


**Fig. 7.** Carrier transport mechanism of LRS (a) from 0.14 V–0.36 V (Frenkel–Poole emission) and (b) from 0.4 V–0.76 V (SCLC); insets show diagram of band bending and carrier transportation for respective mechanism.

## References


[1] S. Tiwari, F. Rana, K. Chan, H. Hanafi, W. Chan, D. Buchanan, in: IEEE International Electron Devices Meeting, 1995, p. 521.
[2] T.C. Chang, S.T. Yan, P.T. Liu, C.W. Chen, S.H. Lin, S.M. Sze, Electrochem. Solid-State Lett. 7 (1) (2004) G17.
[3] W.R. Chen, T.C. Chang, P.T. Liu, P.S. Lin, C.H. Tu, C.Y. Chang, Appl. Phys. Lett. 90 (2007) 112108.
[4] Ting-Chang Chang, Fu-Yen Jian, Shih-Cheng Chen, Yu-Ting Tsai, Mater. Today 14 (12) (2011) 608.
[5] H.Y. Lee, P.S. Chen, T.Y. Wu, Y.S. Chen, C.C. Wang, P.J. Tzeng, C.H. Lin, F. Chen, C.H. Lien, M.-J. Tsai, IEDM Tech. Dig., 1, 2008.
[6] Y.E. Syu, T.C. Chang, T.M. Tsai, Y.C. Hung, K.C. Chang, M.J. Tsai, M.J. Kao, S.M. Sze, IEEE Electron Device Lett. 32 (4) (2011) 545.
[7] Y.T. Tsai, T.C. Chang, C.C. Lin, S.C. Chen, C.W. Chen, S.M. Sze, F.S. Yeh (Hung), T.Y. Tseng, Electrochem. Solid-State Lett. 14 (3) (2011) H135.
[8] Kyung Min Kim, Byung Joon Choi, Bon Wook Koo, Seol Choi, Doo Seok Jeong, Cheol Seong Hwang, Electrochem. Solid-State Lett. 9 (12) (2006) G343.
[9] Chih-Yang Lin, Chen-Yu Wu, Chung-Yi Wu, Chenming Hu, Tseung-Yuen Tseng, J. Electrochem. Soc. 154 (9) (2006) G189.
[10] M.J. Lee, Y. Park, S.E. Ahn, B.S. Kang, C.B. Lee, K.H. Kim, W.X. Xianyu, I.K. Yoo, J.H. Lee, S.J. Chung, Y.H. Kim, C.S. Lee, K.N. Choi, K.S. Chung, Appl. Phys. Lett. 86 (2004) 013502.
[11] Heng Yuan Lee, Pang Shiu Chen, Tai Yuan Wu, Ching Chiun Wang, Pei Jer Tzeng, Cha Hsin Lin, Frederick Chen, Ming-Jinn Tsai, Chenhsin Lien, Appl. Phys. Lett. 92 (2008) 142911.
[12] Min Kyu Yang, Jae-Wan Park, Tae Kuk Ko, Jeon-Kook Lee, Appl. Phys. Lett. 95 (2009) 042105.
[13] Nuo Xu, Lifeng Liu, Xiao Sun, Xiaoyan Liu, Dedong Han, Yi Wang, Ruqi Han, Jinfeng Kang, Bin Yu, Appl. Phys. Lett. 92 (2008) 232112.
[14] H.Y. Peng, G.P. Li, J.Y. Ye, Z.P. Wei, Z. Zhang, D.D. Wang, G.Z. Xing, T. Wu, Appl. Phys. Lett. 96 (2010) 192113.
[15] M.C. Chen, T.C. Chang, C.T. Tsai, S.Y. Huang, S.C. Chen, C.W. Hu, S.M. Sze, M.J. Tsai, Appl. Phys. Lett. 96 (2010) 262110.
[16] M.C. Chen, T.C. Chang, S.Y. Huang, S.C. Chen, C.W. Hu, C.T. Tsai, Simon M. Sze, Electrochem. Solid-State Lett. 13 (6) (2010) H191.
[17] F. De Stefano, M. Houssa, J.A. Kittl, M. Jurczak, V.V. Afanas'ev, A. Stesmans, Appl. Phys. Lett. 100 (2012) 142102.
[18] Y.T. Tsai, T.C. Chang, W.L. Huang, C.W. Huang, Y.E. Syu, S.C. Chen, S.M. Sze, M.J. Tsai, T.Y. Tseng, Appl. Phys. Lett. 99 (2011) 092106.
[19] P.C. Yang, T.C. Chang, S.C. Chen, Y.S. Lin, H.C. Huang, D.S. Gan, Electrochem. Solid-State Lett. 14 (2) (2011) H93.
[20] Simon M. Sze, Kwok K. Ng, Physics of Semiconductor Devices, third ed. Wiley-Interscience, 2006.
[21] D.C. Kim, S. Seo, S.E. Ahn, D.-S. Suh, M.J. Lee, B.-H. Park, I.K. Yoo, I.G. Baek, H.-J. Kim, E.K. Yim, J.E. Lee, S.O. Park, H.S. Kim, U-In Chung, J.T. Moon, B.I. Ryu, Appl. Phys. Lett. 88 (2006) 202102.